

ANNEX C

*Indexes and estimation techniques***Cultural and creative sectors (CCS) and occupations****Table C.1. Cultural and creative sectors included in CCS**

| NACE Rev. 2 industry code | Industry title |
|---------------------------|--|
| 18 | Printing and reproduction of recorded media |
| 32.12 and 32.2 | Manufacture of jewellery and related articles and manufacture of musical instruments |
| 47.61-63 | Retail sale of books, newspapers and stationery, music and video recordings in specialised stores |
| 58.11 and 58.13-14 | Book publishing and publishing of newspapers, journals and periodicals |
| 58.21 | Publishing of computer games |
| 59 | Motion picture, video and television programme production, sound recording and music publishing activities |
| 60 and 63.91 | Programming and broadcasting activities and news agency activities |
| 71.11 | Architectural activities |
| 74.1-3 | Specialised design, photographic, translation and interpretation activities |
| 77.22 | Renting of video tapes and disks |
| 90 | Creative, arts and entertainment activities |
| 91 | Libraries, archives, museums and other cultural activities |

Source: Adapted from Eurostat.

Table C.2. **Cultural occupations included in CCS employment statistics**

| ISCO-08 occupation code | Occupation title |
|-------------------------|---|
| 216 | Architects, planners, surveyors and designers |
| 2353-55 | Other language, music and arts teachers |
| 262 | Librarians, archivists and curators |
| 264 | Authors, journalists and linguists |
| 265 | Creative and performing artists |
| 3431-32 | Photographers and interior designers and decorators |
| 3433 | Gallery, museum and library technicians |
| 3435 | Other artistic and cultural associate professionals |
| 3521 | Broadcasting and audio-visual technicians |
| 4411 | Library clerks |
| 7312 | Musical instrument makers and tuners |
| 7313-14 | Jewellery and precious-metal, potters and related workers |
| 7315 | Glass makers, cutters, grinders and finishers |
| 7316 | Sign writers, decorative painters, engravers and etchers |
| 7317-19 | Handicraft workers in wood, basketry, textile, leather and those not elsewhere classified |

Source: Eurostat.

Methodology to estimate the share of green areas in FUA urban centres

The share of green areas in FUAs is estimated at the urban centre level, using ESA Worldcover data (Zanaga et al., 2021[1]), which provides worldwide land cover data for 2020 at a 10 m resolution. Green areas are defined by the following classes: trees, shrublands and grasslands.

Methodology to estimate the urban heat island intensity

The measure for urban heat island intensity in OECD FUAs was adapted from Chakraborty and Lee (Chakraborty and Lee, 2019[2]). The suggested methodology is composed of the following steps:

1. Define for each FUA using MODIS yearly land cover data (Friedl and Sulla-Menashe, 2019[3]) “urban” and “non-urban” lands, where “urban” refers to the “urban and built-up lands” class in the International Geosphere-Biosphere Programme (IGBP) classification, and “non-urban” to the remaining classes except “water bodies”.
2. By using the ALOS World 3D (Tadono et al., 2014[4]) digital elevation model (DEM), compute elevation statistics for “urban” and “non-urban” lands to ensure elevation patterns are similar in both contexts.
3. Compute land surface temperature using MODIS Terra (Wan, Hook and Hulley, 2015[5]) and Aqua (Wan, Hook and Hulley, 2021[6]) land surface temperature (LST) daily dataset:
 - a. Apply quality filters to remove clouds and ensure an average LST error $\leq 3K$.
 - b. Compute mean temperature in both zones described above. For the “non-urban” land, only pixels with similar elevation statistics as the “urban” area were considered, namely in the range $[z - 2\sigma_z, z + 2\sigma_z]$, where z is the elevation in the “urban” area.
 - c. Compute this mean temperature for the whole year, summer and winter. Summer is defined as 1 June to 31 August for the Northern Hemisphere, and 1 December to 28 February for the Southern hemisphere. Winter is defined reciprocally.

4. Finally, the urban heat island intensity is defined as the temperature difference $T_u - T_r$.

Methodology to estimate soil moisture anomaly

Water content in the superficial layers of the soil is important for water supply and vegetation health. Soil moisture anomaly is a suitable indicator for monitoring the intensity of agricultural droughts. This publication measures agricultural droughts in terms of cropland soil moisture anomaly using the Copernicus Climate Data Store ERA5-Land monthly average data product (European Centre for Medium-range Weather Forecasts, 2022[7]). It is a global gridded product with a 0.1° spatial resolution (~ 11.1 km) from 1950 to the present and provides land variables related to the energy and water cycles over several decades. It contains per-pixel information of the monthly average volume of water in the surface soil layer of 0 to 7 cm deep, expressed as m^3 of water per m^3 of soil. The Copernicus annual 300 m land cover (CCI-LC) (European Space Agency Climate Change Initiative, 2019[8]) enables to get cropland boundaries. Cropland here includes: cropland, rainfed, irrigated or post-flooding; mosaic cropland (>50%)/ natural vegetation (tree, shrub, herbaceous cover) (<50%); and mosaic natural vegetation (tree, shrub, herbaceous cover) (>50%)/cropland (<50%). Once soil moisture grid cells for each year are selected based on cropland land cover, cropland soil moisture anomaly is obtained by computing the percentage change based on the reference period (1981-2010).

Methodology to estimate public transport accessibility

Public transport accessibility is measured using Open Street Map (OSM) (Haklay and Weber, 2008[9]) to get public transport stops. Because of the lack of reliability of OSM in small cities, this publication only focuses on the largest FUA of each OECD country. The Mapbox isochrone API (Mapbox, 2022[10]) then enables to compute isochrones from these public transport stops to get to all the areas located within 10-min walking distance. The Global Human Settlement Population layer 2015 then enables to get the share of the population in each FUA who has access to public transport in less than a 10-min walk.

Methodology to estimate exposure to wildfires

Burnt area by land cover was obtained using JRC's Global wildfire dataset for the analysis of fire regimes and fire behaviours (Artes Vivancos et al., 2019[11]), based on MODIS burned area product Collection 6. This dataset provides monthly individual fire perimeters for 2001-20. Burnt areas are aggregated at the yearly level and then crossed with Copernicus annual 300 m land cover (CCI-LC) data (European Space Agency Climate Change Initiative, 2019[8]).

Population exposure to wildfires over 2010-20 was computed by merging monthly wildfire perimeters and by then taking a 5 km buffer. The Global Human Settlement Population layer for 2015 (Schiavina, Freire and MacManus, 2019[12]) enabled then to compute the population exposed to at least one fire over 2010-20.

Methodology to estimate exposure to river floods

Population exposure to river floods was estimated using the River Flood Hazard Maps at European and Global Scale (Dottori et al., 2021[13]). For OECD countries located in Europe and the Mediterranean Basin, the regional map was used, as the spatial granularity is 250 m. For the remaining OECD countries, the global map with a spatial granularity of 1 km was used. These datasets identify flooded areas for river flood events of different return periods (10 to 500 years). A return period refers to the estimated time interval between floods of similar intensity. Here a return period of 100 years is considered. The 100-year return period is calculated based on past events but the frequency of such climate-related disasters is likely to increase. Changes in flood risk are unevenly

distributed, with the largest increases in America, Asia and Europe but without higher flood protection standards, flood events are projected to rise in all continents. Therefore, 100-year floods are likely to happen more often going forward.

Methodology to estimate population exposure to heat stress

Population exposure to heat stress was estimated using the Universal Thermal Comfort Index (UTCI). The UTCI considers air temperature, wind, radiation and humidity and enables to assess the impact of atmospheric conditions on the human body: $32^{\circ}\text{C} < \text{UTCI} < 38^{\circ}\text{C}$ is considered as strong heat stress, $38^{\circ}\text{C} < \text{UTCI} < 46^{\circ}\text{C}$ as very strong heat stress, and $\text{UTCI} > 46^{\circ}\text{C}$ as extreme heat stress.

The Copernicus Climate Data Store provides hourly thermal comfort indices grids derived from ERA5 reanalysis (CDS, 2022[14]). The spatial resolution is $0.25^{\circ}\times 0.25^{\circ}$. To obtain the population exposure to strong heat stress, we applied the following steps:

- Compute daily maximum UTCI grids.
- Apply a threshold of 32°C on these daily masks and sum by year to get yearly grids of the number of days of strong heat stress or worse.
- Compute by large region zonal statistics weighted by population by using the GHSL-POP layers.
- Consider 1981-2010 as the reference period to get the reference average number of days of strong heat stress and compare this value with recent years.

Methodology to estimate electricity indicators at the regional level

To estimate the electricity indicators at the regional level, the Global Power Plant Database (GPPD) (Byers et al., 2021[15]), the International Energy Agency (IEA) electricity and heat database (OECD, 2022[16]) and the harmonised global dataset of wind and solar farm (GWS) locations and power (Dunnett et al., 2020[17]) are used.

The GPPD provides information on power plants located in 167 countries all over the world, including the 38 OECD countries. For each power plant, the GPPD provides the geographic co-ordinates and the following attributes:

- The energy source: oil, gas, coal, petroleum coke, cogeneration, hydro, wind, waste, biomass, wave and tidal, geothermal, solar, nuclear and others.
- The generation capacity, which is the maximum power (in megawatts, MW) that the plant can deliver. The capacity is a facility-specific characteristic and does not change over time, unless extension or upgrade of the power station, or a shutdown of a part of it.
- The annual electricity generation, which provides the amount of electricity generated over a year (in GWh). This indicator is reported over the period 2013-19. When no electricity generation was reported, the annual electricity generation was estimated. The annual generation corresponds to the gross generation, i.e. the electricity consumption of the power plant for its operation is not deducted.
- The country where the power plant is registered.

As the coverage of wind and solar power plants in the GPPD was not satisfying, the GWS farm locations and power was used instead to get the locations of wind and solar power sources.

The International Energy Agency (IEA (IEA, 2022[18])) database includes national-level electricity generation data by energy source for most OECD countries. The IEA dataset used to estimate electricity generation indicators at the local level corresponds to the gross electricity production by energy source in 2019. A breakdown of 53 different sources is available.

Electricity generation estimates

In order to remain consistent across countries and energy sources, electricity generation was estimated at the power plant level based on the relative capacity of each power plant (from the GPPD and GWS) and on the total national electricity generation from each energy source (from the IEA). The methodology follows the four steps below:

1. Map energy sources from the IEA to the GPPD classification.

The IEA electricity production data provides a higher level of detail in terms of breakdown by energy source compared to the GPPD data. For this reason, each energy source type recorded in the IEA database was matched to a source category in the GPPD.

2. Determine the share of national capacity for each power plant.

For each power plant p , located in the country c and generating electricity from the energy source f , the share of the capacity of the power plant in the national capacity for the source f is calculated as:

$$share_{p,c,f} = \frac{capacity_{p,c,f}}{\sum_i capacity_{i,c,f}}$$

where $i \in$ power plants located in the country c , and generating electricity from the source f .

3. Allocate a part of the national generation to each power plant.

For each power plant p , generating electricity from source f , in the country c , the estimated generation is calculated as:

$$generation_{p,c,f} = share_{p,c,f} * national\ generation_{c,f}$$

Aggregation at local scales

To compute indicators at different geographical scales, a point shapefile was created from the GPPD and GWS databases using the latitude and longitude provided for each facility – each point representing a power plant. The point shapefile was overlapped with two other shapefiles corresponding to the boundaries of the subnational geographies available in OECD countries (TL2 and TL3 regions). Thus, each power plant can be associated to a TL2 region and a TL3 region. Offshore power plants were assigned to the closest region (of the registered host country) based on the distance to the coast.

Year of reference

All indicators presented in this document refer to the year 2019, which corresponds to the latest year for which capacity data is available in the GPPD.

Breakdown by energy source categories

The GPPD includes 13 different energy sources. These energy sources were aggregated into 6 categories (coal, gas, oil, nuclear, renewables and others). The energy sources within each category are comparable in terms of technology, risks and impacts on the environment.

Electricity generation indicators

For each region r , generation data was aggregated into each category i as:

$$generation_{r,i} = \sum_{k \in i} power\ plant\ generation_{r,k}$$

where $k \in \{\text{coal, gas, oil, petroleum coke, cogeneration, nuclear, hydro, wind, waste, biomass, wave, geothermal, solar}\}$, $i \in \{\text{coal, gas, oil, nuclear, renewables and others}\}$, and $power\ plant\ generation_{r,k}$ is the electricity generation of a power plant located in the region r , generating electricity from the source type k .

Energy mix indicators

For each region r , the share of each energy source category i is calculated as:

$$share_{r,i} = \frac{generation_{r,i}}{\sum_j generation_{r,j}} * 100$$

where $j \in \{\text{coal, gas, oil, nuclear, renewables, others}\}$.

Greenhouse gas (GHG) emissions from electricity generation indicators

GHG emissions indicators are derived from both the electricity generation by energy source and the emission factors for each energy source. Electricity generation was estimated at the power plant level for each energy source included in the GPPD as described above. Emission intensity by energy source comes from the IPCC estimates on GHG emissions of supply technologies.

For each region r , the GHG emissions (in tons of CO₂ equivalent) are calculated as:

$$emissions_r = \sum_{k \in f} generation_{r,k} * emission_intensity_k$$

where the emission intensity corresponds to the median value of the lifecycle emissions (in gCO₂eq/kWh), $f \in \{\text{coal, gas, oil, petroleum coke, cogeneration, nuclear, hydro, wind, waste, biomass, wave, geothermal, solar}\}$.

Emission intensity

For each region r , the emission intensity (in tons of CO₂ equivalent per GWh) is calculated as:

$$emission_intensity_r = \frac{emissions_r}{\sum_i generation_{r,i}}$$

where $i \in \{\text{coal, gas, oil, nuclear, renewables and others}\}$.

Methodology to estimate GHG emissions by sector

GHG emissions at the subnational level were estimated using the Emissions Database for Global Atmospheric Research (EDGAR) (Crippa et al., 2021[19]), version 6.0 of the EC JRC. EDGAR provides annual sector-specific grid maps for the three main GHGs (CO₂, CH₄, and N₂O) at a 0.1° spatial resolution (~11 km). Other GHGs, such as fluorinated gases, are not available at the moment. The different sectors and subsectors covered are:

- **Energy industry:**
 - **Energy production:** Power industry (IPCC 2006: 1A1a).
 - **Energy transformation:** Oil refineries and transformation industry (1A1b, 1A1ci, 1A1cii, 1A5biii; 1B1b, 1B2aiii6, 1B2biii3, 1B1c).
 - **Energy extraction:** Fuel exploitation (oil, coal, natural gas) (1B1a, 1B2aiii2, 1B2aiii3, 1B2bi, 1B2bii).
- **Manufacturing industry:** Combustion for manufacturing (1A2), chemical processes (2B), iron and steel production (2C1, 2C2), non-ferrous metals production (2C3 to 2C7), non-energy use of fuels (2D1, 2D2, 2D4), solvents and products use (2D3, 2E, 2F, 2G), non-metallic minerals production (2A), oil refineries and transformation industry (1A1b, 1A1ci, 1A1cii, 1A5biii; 1B1b, 1B2aiii6, 1B2biii3, 1B1c).
- **Buildings:** Energy for buildings (1A4+1A5).
- **Waste:** waste water handling (4D), solid waste landfills (4A+4B), solid waste incineration (4C).
- **Transport:** Road transportation (1A3b), aviation (1A3a), shipping (1A3d), railways, pipelines, off-road transport (1A3c+1A3e).

- **Agriculture:** Enteric fermentation (3A1), manure management (3A2), agricultural waste burning (3C1b), agricultural soils (3C2+3C3+3C4+3C7), indirect N₂O emissions from agriculture (3C5+3C6).
- **Other:** Fossil fuel fires (5B), indirect emissions from NO_x and NH₃ (5A).

Emissions from Land Use and Land Cover Change (LULCC) are not included. National GHG emissions are disaggregated by using subsector-specific geospatial proxies. For example, the road transport emissions estimates are based on different types of road networks extracted from Open Street Map (Haklay and Weber, 2008[9]) (highways, primary and secondary, residential and commercial roads) and different weighting factors for each road type. Road traffic is not directly considered. For more details about the disaggregation methodology, refer to the *OECD Regional Outlook 2021* (OECD, 2021[20]).

GHG emissions are expressed in CO₂ equivalents using 100-year global warming potential from the IPCC 5th Assessment Report (AR5), i.e. 28 for CH₄, and 265 for N₂O.

Methodology to estimate emissions from key manufacturing sectors

European Union Emission Trading System (EU-ETS, 2020[21]) emissions and ORBIS (Pinto Ribeiro, Menghinello and De Backer, 2010[22]) data were used to estimate emissions in key manufacturing sectors. EU-ETS emissions data cover high emissions installations and provide the exact location of each installation. They cover most emissions in refined petroleum and coke, chemicals, basic metals and other non-metallic minerals. However, publicly available ETS emissions data provide limited information on the sectoral origin of emissions within manufacturing and this information does not follow NACE sectors. Most ETS emissions are attributed to fuel combustion with no breakdown. ETS emissions have been mainly attributed to NACE sectors according to the main activity of businesses owning installations using ORBIS business data.

For more details on the methodology, refer to *Regional Industrial Transitions to Climate Neutrality: Identifying vulnerable regions* (OECD, forthcoming[23]).

Methodology to estimate regional energy intensity in European large regions

Regional energy intensity estimates were obtained using the following Eurostat datasets:

- Energy supply and use by NACE Rev. 2 activity (env_ac_pefasu) (Eurostat, 2022[24]).
- SBS data by NUTS 2 regions and NACE Rev. 2 (from 2008 onwards) (sbs_r_nuts06_r2) (Eurostat, 2021[25]).

National energy consumption data by NACE sector for European countries provided in env_ac_pefasu were disaggregated using the NUTS-2 employment data by NACE sector given in sbs_r_nuts06_r2.

Methodology to estimate land use in cities

Land use in cities was estimated by using publicly available satellite imagery (Sentinel-1 and -2) and a Deep Learning image segmentation model (U-Net). The model was trained on the Copernicus Urban Atlas (EEA, 2020[26]) to automatically detect land use patterns on satellite images aggregated at the yearly level. Population estimates are obtained using the GHSL-POP layer (2022 release) for 2020

(JRC, 2022[27]). For more details on the methodology, refer to “Monitoring land use in cities using satellite imagery and deep learning” (Banquet et al., 2022[28]).

Methodology to estimate the potential for remote working

The assessment of regions’ capacity to adapt to remote working is based on the diversity of tasks performed in different types of occupations and is structured in two steps.

The first step requires classifying each occupation based on the tasks required and according to the degree to which those tasks can be performed remotely. Such a classification is based on a recent study by Dingel and Neiman (2020[29]), which is built from the O*NET surveys conducted in the United States. The second step relies on data from labour force surveys and consists of assessing the geographical distribution of different types of occupations and subsequently matching those occupations with the classification performed in the first step. Combining the two data sets allows for assessing the number of workers who can perform their tasks from home as a share of the total employment in the region.

This assessment does not consider the specific regulations or arrangements that each country applies to remote working and which affect the actual share of people working remotely. For example, limitations in the days of remote working for cross-border workers are not reflected in the estimates presented here.

Theil entropy index

Definition

Regional disparities are also measured by a Theil entropy index, which is defined as:

$$Theil = \sum_{i=1}^N \frac{y_i}{\bar{y}} \ln\left(\frac{y_i}{\bar{y}}\right)$$

where N is the number of regions in the OECD, y_i is the variable of interest in the i^{th} region (i.e. household income, life expectancy, homicide rate, etc.) and \bar{y} is the mean of the variable of interest across all regions.

The Theil index can be easily decomposed into two components: i) the disparities within subgroups of regions – where for example a subgroup is identified by a set of regions belonging to a country; ii) the disparities between subgroups of regions (i.e. between countries). The sum of these two components is equal to the Theil index.

In order to decompose the Theil index, let us start by assuming m groups of regions (countries). The decomposition will assume the following form:

$$Theil = \sum_{j=1}^M \sum_{i=1}^N s_j \frac{y_{ij}}{\bar{y}_j} \ln\left(\frac{y_{ij}}{\bar{y}_j}\right) + \sum_{j=1}^M s_j \ln\left(\frac{\bar{y}_j}{\bar{y}}\right)$$

where the first term of the formula is the *within* part of the decomposition equal to the weighted average of the Theil inequality indexes of each country. Weights, s_j , are computed as the ratio between the country average of the variable of interest and the OECD average of the same variable. The second term is the *between* component of the Theil index and represents the share of regional disparities that depends on the disparities across countries.

Interpretation

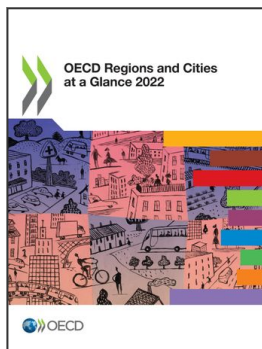
The Theil index ranges between zero and ∞ , with zero representing an equal distribution and higher values representing a higher level of inequality.

The index assigns equal weight to each region regardless of its size; therefore, differences in the values of the index among countries may be partially due to differences in the average size of regions in each country.

References

- [11] Artes Vivancos, T. et al. (2019), "A global wildfire dataset for the analysis of fire regimes and fire behaviour", *Scientific Data*, Vol. 6, p. 296.
- [28] Banquet, A. et al. (2022), "Monitoring land use in cities using satellite imagery and deep learning", *OECD Regional Development Papers*, No. 28, OECD Publishing, Paris, <https://doi.org/10.1787/dc8e85d5-en>.
- [15] Byers, L. et al. (2021), *A Global Database of Powerplants*, <https://www.wri.org/publication/global-power-plant-database>.
- [14] CDS (2022), *Thermal Comfort Indices Derived from ERA5 Reanalysis*, Copernicus Climate Change Service Climate Data Store, <https://cds.climate.copernicus.eu/cdsapp#!/dataset/derived-utci-historical?tab=overview>.
- [2] Chakraborty, T. and X. Lee (2019), "A simplified urban-extent algorithm to characterize surface urban heat islands on a global scale and examine vegetation control on their spatiotemporal variability", *International Journal of Applied Earth Observation and Geoinformation*, Vol. 74, pp. 269-280, <https://doi.org/10.1016/j.jag.2018.09.015>.
- [19] Crippa, M. et al. (2021), *EDGAR v6.0 Greenhouse Gas Emissions*, Joint Research Centre (JRC), European Commission, <http://data.europa.eu/89h/97a67d67-c62e-4826-b873-9d972c4f670b>.
- [29] Dingel, J. and B. Neiman (2020), "How many jobs can be done at home?", *Becker Friedman Institute White Paper March*, <https://bfi.uchicago.edu/working-paper/how-many-jobs-can-be-done-at-home/>.
- [13] Dottori, F. et al. (2021), "River flood hazard maps for Europe and the Mediterranean Basin region", Joint Research Centre (JRC), European Commission.
- [17] Dunnett, S. et al. (2020), "Harmonised global datasets of wind and solar farm locations and power", *Scientific Data*, Vol. 7/1, p. 190, <https://doi.org/10.1038/s41597-020-0469-8>.
- [26] EEA (2020), *Urban Atlas LCLU 2018*, European Environment Agency, <https://land.copernicus.eu/local/urban-atlas/urban-atlas-2018>.
- [21] EU-ETS (2020), *Verified Emissions for 2019*, European Union Emission Trading System, https://ec.europa.eu/clima/eu-action/eu-emissions-trading-system-eu-ets/union-registry_en#ecl-inpage-1121.
- [7] European Centre for Medium-range Weather Forecasts (2022), *ERA5-Land Monthly Averaged Data from 1950 to Present*, <https://cds.climate.copernicus.eu/cdsapp#!/dataset/reanalysis-era5-land-monthly-means?tab=overview>.
- [8] European Space Agency Climate Change Initiative (2019), *Land Cover Classification Gridded Maps from 1992 to Present Derived from Satellite Observations*.
- [24] Eurostat (2022), *Energy Supply and Use by NACE Rev. 2 Activity*, https://ec.europa.eu/eurostat/databrowser/view/env_ac_pefasu/default/table?lang=en.
- [25] Eurostat (2021), *Structural Business Statistics Data by NUTS 2 Regions and NACE Rev. 2 (from 2008 onwards)*, https://appsso.eurostat.ec.europa.eu/nui/show.do?dataset=sbs_r_nuts06_r2&lang=en.
- [3] Friedl, M. and D. Sulla-Menashe (2019), *MCD12Q1 MODIS/Terra+Aqua Land Cover Type Yearly L3 Global 500m SIN Grid V006*. NASA EOSDIS Land Processes DAAC, NASA EOSDIS Land Processes DAAC.
- [9] Haklay, M. and P. Weber (2008), "OpenStreetMap: User-generated street maps", *IEEE Pervasive Computing*, Vol. 7, pp. 12-18.
- [18] IEA (n.d.), "OECD - Electricity and heat generation", *IEA Electricity Information Statistics*, <https://doi.org/10.1787/data-00457-en> (accessed on 24 October 2022).
- [27] JRC (2022), *GHSL Data Package 2022: Public Release GHS P2022*, European Commission Joint Research Centre, <https://data.europa.eu/doi/10.2760/19817>.
- [10] Mapbox (2022), *Isochrone API*, <https://docs.mapbox.com/api/navigation/isochrone/>.
- [16] OECD (2022), "OECD - Electricity/heat supply and consumption", *IEA Electricity Information Statistics*, OECD, Paris, <https://doi.org/10.1787/e2da2a08-en> (accessed on 13 October 2022).
- [23] OECD (2022), *Regional Industrial Transitions to Climate Neutrality: Identifying vulnerable regions*, OECD Publishing, Paris.

- [20] OECD (2021), *OECD Regional Outlook 2021: Addressing COVID-19 and Moving to Net Zero Greenhouse Gas Emissions*, OECD Publishing, Paris, <https://doi.org/10.1787/17017efe-en>.
- [22] Pinto Ribeiro, S., S. Menghinello and K. De Backer (2010), "The OECD ORBIS Database: Responding to the Need for Firm-Level Micro-Data in the OECD", *OECD Statistics Working Papers*, No. 2010/1, OECD Publishing, Paris, <https://doi.org/10.1787/5kmhds8mzj8w-en>.
- [12] Schiavina, M., S. Freire and K. MacManus (2019), "GHS population grid multitemporal (1975, 1990, 2000, 2015)".
- [4] Tadono, T. et al. (2014), "Precise Global DEM Generation By ALOS PRISM, ISPRS Annals of the Photogrammetry", *Remote Sensing and Spatial Information Sciences*, Vol. II-4, pp. 71-76.
- [6] Wan, Z., S. Hook and G. Hulley (2021), *MODIS/Aqua Land Surface Temperature/Emissivity Daily L3 Global 1km SIN Grid V061*.
- [5] Wan, Z., S. Hook and G. Hulley (2015), *MOD11A1 MODIS/Terra Land Surface Temperature/Emissivity Daily L3 Global 1km SIN Grid V006*.
- [1] Zanaga, D. et al. (2021), *ESA WorldCover 10 m 2020 v100*, <https://doi.org/10.5281/zenodo.5571936>.



From:
OECD Regions and Cities at a Glance 2022

Access the complete publication at:
<https://doi.org/10.1787/14108660-en>

Please cite this chapter as:

OECD (2022), "Indexes and estimation techniques", in *OECD Regions and Cities at a Glance 2022*, OECD Publishing, Paris.

DOI: <https://doi.org/10.1787/bcf1f6fa-en>

This work is published under the responsibility of the Secretary-General of the OECD. The opinions expressed and arguments employed herein do not necessarily reflect the official views of OECD member countries.

This document, as well as any data and map included herein, are without prejudice to the status of or sovereignty over any territory, to the delimitation of international frontiers and boundaries and to the name of any territory, city or area. Extracts from publications may be subject to additional disclaimers, which are set out in the complete version of the publication, available at the link provided.

The use of this work, whether digital or print, is governed by the Terms and Conditions to be found at <http://www.oecd.org/termsandconditions>.